ELSEVIER

UV-illumination and Au-nanoparticles enhanced gas sensing of *p*-type Na-doped ZnO nanowires operating at room temperature

Cheng-Liang Hsu[a],*, Bo-Yu Jhang[a], Cheng Kao[a], Ting-Jen Hsueh[b]

[a] *Department of Electrical Engineering, National University of Tainan, Tainan, 700, Taiwan, ROC*
[b] *Department of Electronic Engineering, National Kaohsiung University of Science and Technology, Kaohsiung, 807, Taiwan, ROC*

ABSTRACT

High density *p*-type Na-doped ZnO nanowires were uniformly grown on glass substrate via the hydrothermal method, and then examined by SEM, XRD, PL, XPS, and TEM analysis. The *p*-type characteristic of the nanowires was verified through Hall and humidity measurements. $2 \sim 6$ nm Au nanoparticles were sputtered on the nanowires to fabricate a room temperature sensor and strengthen its *p*-type property, which was enhanced by the Schottky barrier at Au NPs/ZnO interface. The *p*-type gas sensor has a high response, sensitivity and selectivity under UV illumination at room temperature.

1. Introduction

Metal oxide (MO) gas sensors are applied to internet of things (IoT) devices, military equipment, and industrial and environmental monitoring tools [1,2], owing to their quick response and high sensitivity [3]. MO gas sensors can have a functional lifetime surpassing 15 years, which is much longer than organic gas sensors. Additionally, the size of MO gas sensors have shrunk to the micro- and nano-scale by micro-electromechanical systems (MEMS) technology and semiconductor fabrication processes [4]. As such, these tiny sensors can now be embedded in wearables and smart phones for increasing the value of portable electronic products. The disadvantage of MO gas sensors, however, is the high working temperatures $250 \sim 450\,°C$ [5], which requires high power consumption with most of the energy lost through heat due to the sensing response of MO gas sensors being related to gaseous species chemisorption and reaction at high working temperatures. Currently, there are several methods to decrease the operating temperature while increasing the gas-sensing performance [4,6–10], including doping various elements, decorating with noble metal nanoparticles (NPs), shrinking the sensor to the micro- and nano-scale, applying an electrostatic field, and ultraviolet (UV) illumination, among others.

The *n*-type and *p*-type properties of MO materials are important for the gas-sensing response, selectivity and sensor-array assembly. The common gas sensor of MO materials (such as Sn_2O_3, ZnO, TiO_2, In_2O_3, and their compounds) is usually derived from the *n*-type property [11–14]; nevertheless, a few *p*-type MO gas sensors (such as CuO and

NiO) have been investigated and reported [15,16]. The advantages of *p*-type volatile organic compound (VOC) sensors in comparison to *n*-type ones [17], such as higher thermal stability, lower humidity dependence, faster recovery kinetics, thermal operation stability, potential applied in *p–n* homojunction and heterojunction. In recent years, gas sensors employing ZnO nanostructures (NSs) have attracted much attention due to their novel chemical absorption and reactive properties [18], which are attributed by their nanoscale size and large surface area to volume ratio. ZnO is a native *n*-type semiconductor and difficult to change to the *p*-type property. Currently, the *p*-type ZnO is usually created by doping with a V-group (N, P, As, or Sb) element [7,13]. In this investigation, a novel *p*-type gas sensor has been simply fabricated by Na-doped ZnO (ZnO:Na) nanowires (NWs) decorated with Au NPs. The proposed sensor uses a glass substrate, which is easier to combine with UV-LED. Under UV illumination, this sensor can be operated at room temperature for low power consumption. Details of the Au NPs/*p*-ZnO:Na NWs fabricated on the glass substrate and characteristics of the analysis for humidity and UV light-activated ethanol sensing are discussed.

2. Experimental

Fig. 1 presents a schematic illustration of the Au NPs/*p*-ZnO:Na NWs sensor the measured current-voltage (*I-V*) curves under UV-LED (Nichia) illumination. The glass substrate (size: 1 cm × 1 cm, Corning® Eagle XG) was cleaned with acetone and deionized (DI) water. Radio-frequency (RF) magnetron sputtering was then used to deposit a 30 nm
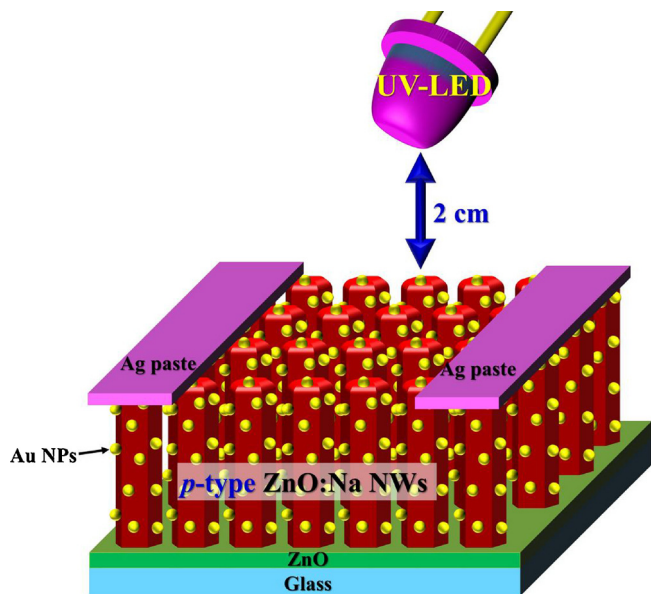

Fig. 1. Schematic diagram of the Au NPs/*p*-ZnO:Na NWs gas sensor measured under UV-LED illumination.

thick ZnO seed layer on the glass substrate. The resistance of the ZnO seed layer is very high ($> 1G\Omega$) due to its highly crystalline structure and ultra-low defect density. Subsequently, the ZnO/glass substrate was immersed in a solution containing 0.02 M sodium nitrate ($NaNO_3$), 0.06 M hexamethylenetetramine ($C_6H_{12}N_4$), and 0.06 M nitrate hexahydrate ($Zn(NO_3)_2 \cdot 6H_2O$). The solution and samples were placed in a sealed autoclave, after which *p*-ZnO:Na NWs were hydrothermally grown on the ZnO/glass substrate at 100 °C over 5 h. The mechanism and equations of the hydrothermal synthesis have been discussed in detail in previous reports [19]. Finally, Au NPs were direct-current (DC) sputtered on the *p*-ZnO:Na NWs for 3 s and then annealed at 200 °C for 6 h.

The morphology, crystallinity, optical characteristics and elemental analysis of the Au NPs/*p*-ZnO:Na NWs were analyzed by field-emission scanning electron microscopy (FE-SEM, JEOL-7000 F), high-resolution transmission electron microscopy (HR-TEM, JEOL-JEM2100 F), X-ray diffraction (XRD, MAC-MXP18), X-ray photoelectron spectroscopy (XPS) (Kratos Axis Ultra DLD) and photoluminescence (PL) spectroscopy (Jobin-Yvon SPEX System). The fabricated sensors were then placed in a sealed chamber to measure the *I-V* curves of humidity and gas sensing by a source meter (Keithley Model-4200) at atmospheric pressure. The electroluminescence (EL) spectra of UV-LED (input 4.3 V and 200 mA) have an obvious strong peak at 368 nm. The UV-LEDs (6 mW/cm^2) were placed at a distance of ~2 cm from the Au NPs/*p*-ZnO:Na NWs sample. Volatile organic compounds (VOCs) were then injected into the chamber for sensing response measurement, after which air was pump into the chamber to decrease the VOCs concentration for sensing recovery measurement.

3. Results and discussion

Figs. 2(a) and (b) display the top view and cross sectional FE-SEM images of the *p*-ZnO:Na NWs grown on the ZnO/glass substrate. The inset image in the top-right-hand corner of Fig. 2(b) is the energy dispersive X-ray (EDX) spectroscopy of the *p*-ZnO:Na NWs. As can be seen, the NWs morphology has uniform growth and good *c*-axis orientation. The average diameter and length of the *p*-ZnO:Na NWs were ~75 nm and ~1.76 μm, respectively. The EDX spectroscopy indicated Zn, O, and Na element signal peaks. The intensity ratio of these signal peaks showed that the Na content in the *p*-ZnO:Na NWs was around ~11.85 atomic %; however, this figure may not be accurate due to the position
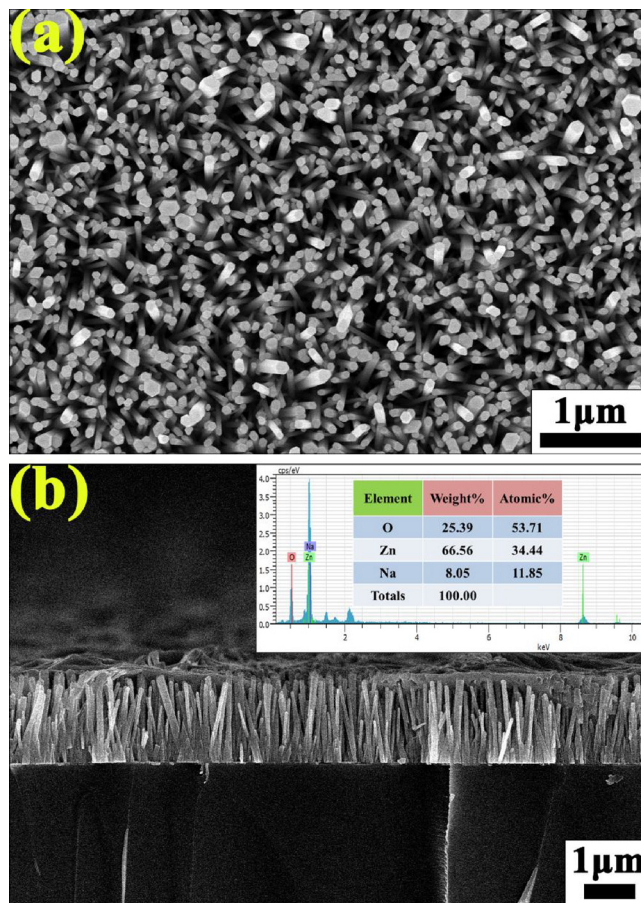

Fig. 2. (a) Top-view and (b) cross-sectional SEM images of the *p*-ZnO:Na NWs/glass; inset image is the EDX spectra.

of the Na signal peak being very near the Zn peak. Moreover, the Na signal peak was affected and superposed by the Zn peak, which indicates that it is difficult to obtain the accurate Na content in the *p*-ZnO:Na NWs.

The XPS of the *p*-ZnO:Na and *n*-ZnO NWs are shown in Fig. 3(a). The XPS spectra of these NWs revealed strong Zn and O peaks, which demonstrates that the major content of these NWs is ZnO; in contrast, the weak Na intensity is attributed to the Na doping being slight. However, Na peak of *p*-ZnO:Na was stronger than *n*-ZnO NWs for demonstrated Na dopant in ZnO. Fig. 3(b) reveals the XRD patterns of the *p*-ZnO:Na and *n*-ZnO NWs, which according to JCPDS card no. 36-1451, are clearly in the ZnO wurtzite crystal phase. The XRD of the *p*-ZnO:Na NWs displays a few small Na_2ZnO_2 peaks, which implies that the *p*-ZnO:Na NWs include a slight amount of Na_2ZnO_2 compound. The reaction kinetics of sodium zincate (Na_2ZnO_2) is as follows:

$$Zn(OH)_2 + 2NaOH \rightarrow Na_2ZnO_2 + 2H_2O$$

$$ZnO + 2NaOH \rightarrow Na_2ZnO_2 + H_2O$$
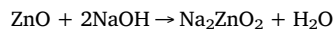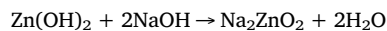
The Na_2ZnO_2 has not observed by HR-TEM image and SAED pattern. The XRD pattern reveals a very small Na_2ZnO_2 phase. Speculated the amount of Na_2ZnO_2 is slight. In the general, the heterojunctions compound has the grain boundary in the interface to affect sensitivity of sensor [13,20]. Assume that ZnO/Na_2ZnO_2 heterojunction should be affected the sensitivity. The inset image of Fig. 3(b) shows that the *p*-ZnO:Na NWs peak is shifted 0.08° to a small angle, which indicates the lattice constant is enlarged due to the Na dopant. Fig. 3(c) displays the PL spectra of the *p*-ZnO:Na and *n*-ZnO NWs. Although the intensity of the near band edge (NBE) peak of the *n*-ZnO NWs is larger than the deep level emissions (DLE) peak, the intensity of NBE peak of *p*-ZnO:Na NWs